Microwave Brightness Temperature Characteristics of Three Strong Earthquakes in Sichuan Province, China

Feng Jing, *Member, IEEE*, Ramesh P. Singh, *Member, IEEE*, Yueju Cui, and Ke Sun

***Abstract*—Passive microwave remote sensing technology is an effective means to identify the thermal anomalies associated with earthquakes due to its penetrating capability through clouds compared with infrared sensors. However, observed microwave brightness temperature is strongly influenced by soil moisture and other surface parameters. In the present article, the segmented threshold method has been proposed to detect anomalous microwave brightness temperature associated with the strong earthquakes occurred in Sichuan province, China, an earthquake-prone area with high soil moisture. The index of microwave radiation anomaly (IMRA) computed by the proposed method is found to enhance prior to the three strong earthquakes, 2008 Wenchuan ($M = 7.8$), 2013 Lushan ($M = 6.6$), and 2017 Jiuzhaigou ($M = 6.5$), occurred during 2008–2018 using the Defense Meteorological Space Program Special Sensor Microwave Imager/Sounder F17 satellite data. Our results show that the microwave brightness temperature anomalies appeared about two months prior to the three strong earthquakes. For the Wenchuan and Lushan earthquakes, the enhanced IMRA distributed along the main fault, which is consistent with the variations of our earlier studies of the 1997 Manyi ($M = 7.5$) and the 2001 Kokoxili ($M = 7.8$) earthquakes in the region with low soil moisture. For the Jiuzhaigou earthquake, the anomalies distributed around the epicenter and do not indicate the seismogenic structure, which could be due to the presence of a blind fault. It should be noted that quantitative evaluation of IMRA is limited due to infrequent occurrence of earthquakes.**

***Index Terms*—Brightness temperature, earthquakes, passive microwave remote sensing, thermal anomalies.**

I. Introduction

LIKE thermal infrared satellite observation, passive microwave remote sensing is an important tool to determine information about the thermal radiations. The possible thermal anomalies prior to the occurrence of earthquakes around the globe have been widely reported using satellite infrared observations since last three decades [1]–[9]. The satellite infrared observations associated with the earthquakes are limited due to cloud cover depending on the weather conditions, although some anomaly detection methods have been proposed to reduce the effects of cloud cover [10], [11]. Recently, variations of microwave brightness temperature at different frequencies with the changes in stress prior to rock rupture have been detected through rock mechanics experiments [12], [13], which have provided a physical foundation for monitoring earthquake activities using passive microwave satellite observation data. Based on the laboratory observations and considering that the microwave observation does not depend on the weather conditions, efforts have been made to study thermal anomalies associated with earthquake activities using passive microwave remote sensing data from the Advanced Microwave Scanning Radiometer for Earth observation system (AMSR-E) and Special Sensor Microwave Imager (SSM/I) [14]–[18]. These observations provided support to believe that passive microwave remote sensing is an effective means for detecting possible thermal anomaly signals associated with the strong earthquakes.

Index of microwave radiation anomaly (IMRA) provides information about the earthquakes occurred in the relatively low soil moisture (SM) and low vegetation cover areas [19]. The distinct microwave brightness temperature enhancements at 19.35 GHz with horizontal polarization have been observed prior to the 1997 Manyi M 7.5 earthquake and the 2001 Kokoxili M 7.8 earthquake [19]. The good correlation between the enhancement of spatial distribution of IMRA and seismogenic fault activities has been observed. However, IMRA proposed by Jing *et al.* [19] does not provide reliable information related to the 2008 Wenchuan M 7.8 earthquake, which is one of the strongest earthquakes in China after the 1976 Tangshan M 7.8 earthquake. In fact, the thermal anomalies associated with the Wenchuan great earthquake have been observed from the satellite infrared observations [16], [20]–[23]. The IMRA associated with the Wenchuan earthquake fails to provide any information that could be related to the high SM in the earthquake preparation region. The relationship between the surface, subsurface, weather factors, and microwave brightness temperature indicated that high SM, vegetation cover, and water vapor, greatly affect microwave brightness temperature [24].

In the present article, we proposed the segmented threshold method to obtain IMRA and identified the potential microwave radiation signals associated with strong earthquakes that occurred in one of the earthquake-prone areas of China with high SM. Microwave brightness temperature data from the Defense Meteorological Space Program (DMSP) Special Sensor Microwave Imager/Sounder (SSMIS) F17 satellite have been selected. Considering the observation period of F17, three

Manuscript received November 5, 2019; revised January 2, 2020; accepted January 18, 2020. Date of publication January 27, 2020; date of current version February 13, 2020. This work was supported in part by the National Natural Science Foundation of China under Grant 41604062 and in part by the Basic Research Project of Institute of Earthquake Forecasting, CEA, under Grant 2017IES0403. *(Corresponding author: Feng Jing.)*

F. Jing, Y. Cui, and K. Sun are with the Institute of Earthquake Forecasting, China Earthquake Administration, Beijing 100036, China (e-mail: jingfeng@cea-ies.ac.cn; cehuicuiyueju@126.com; sunke22@126.com).

R. P. Singh is with the Schmid College of Science and Technology, Chapman University, Orange, CA 92866 USA (e-mail: rsingh@chapman.edu).

This paper has supplementary downloadable multimedia material available at http://ieeexplore.ieee.org provided by the authors.

Digital Object Identifier 10.1109/JSTARS.2020.2968568

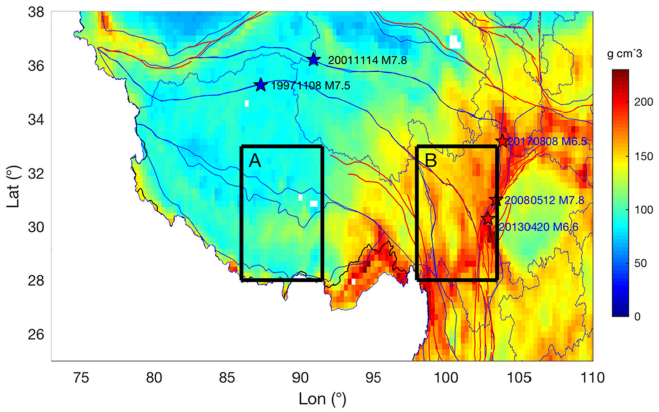

Fig. 1. Two contrasting SM regions in the southwest of China based on AMSR-E observation. Region A (28°–33°N, 86°–91°E) with the lower SM and region B (28°–33°N, 98°–103.5°E) with the higher SM. The blue stars indicate the two strong earthquakes occurred in the low-SM region reported in [19]. The red stars indicate the three strong earthquakes occurred in the high-SM region discussed in this article.

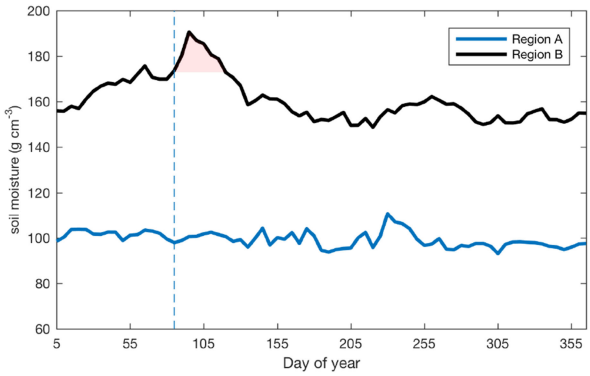

Fig. 2. Daily three-year area-averaged variations of SM for the period 2008–2010 over A and B regions. Blue dash line shows the start of an enhancement of SM over region B. Red shadow shows the range with smaller fluctuations of brightness temperature (see Fig. 4).

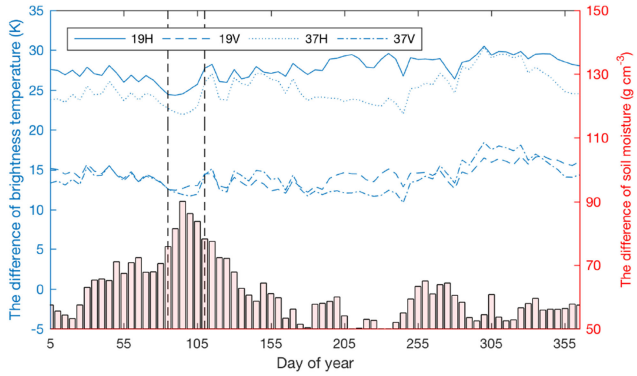

Fig. 3. Difference in SM and in passive microwave brightness temperature at 19 and 37 GHz (horizontal and vertical polarizations) in regions A and B using daily-area-averaged data from 2008 to 2010. The part between the two black dash lines indicates two types of data having a completely opposite variations trend.

earthquakes (magnitude greater than 6.5) occurred during 2008–2018 in Sichuan province of China (Wenchuan, $M = 7.8$ of May 12, 2008, Lushan $M = 6.6$ of April 20, 2013, and Jiuzhaigou $M = 6.5$ of August 8, 2017) have been considered in the present study. Detailed spatial analysis and the long-term (11 years) variations of IMRA over the seismogenic fault zone/epicentral region have been carried out to understand the correlation between seismic and tectonic activities.

II. Seismic Abnormal Signal Detection

The southwest of China is one of the earthquake-prone areas in mainland China. The SM in this region is totally different from west to east (see Fig. 1). The IMRA using microwave brightness temperature shows information about the 1997 Manyi $M = 7.5$ and the 2001 Kokoxili $M = 7.8$ earthquakes prior to their occurrence; these two earthquakes occurred in the low-SM environment (see Fig. 1) [19]. However, the deadly 2008 Wenchuan earthquake occurred in high-SM environment (see Fig. 1), which could obscure microwave seismic signals. To overcome the suppression of IMRA in the high-SM environment, we proposed a new method to identify the possible earthquake thermal anomaly information using microwave brightness temperature.

A. SM and Microwave Brightness Temperature

Ignoring the effect of brightness temperature with latitudes, two regions with same latitudes and different SMs in the southwest of China were considered as sample regions to analyze the influence of SM on passive microwave brightness temperature (see Fig. 1). The microwave brightness temperature dataset observed by DMSP F17 SSMIS has been considered, which include 19.3 GHz vertical (V) and horizontal (H), 22.2 GHz vertical (V), 37.0 GHz vertical (V) and horizontal (H), and 91.7 GHz vertical (V) and horizontal (H) (hereinafter referred to as 19H, 19V, 22V, 37H, 37V, 91H, and 91V) and with a spatial resolution of 25 km. AMSR-E SM data with the same spatial resolution as SSMIS microwave brightness temperature data have been used to set the different SM regions. Region A is located in the low-SM area, and region B sis in high-SM environment. The three-year data observed during the period 2008–2010 were selected to study the effect of SM on microwave brightness temperature due to the overlapping observation periods of SSMIS F17 brightness temperature and AMSR-E SM data.

Detailed analysis has been carried out over region A with low SM and region B with high SM. Fig. 2 shows the daily three-year area-averaged variations of SM for the period 2008–2010 over the two regions. The blue dash line (see Fig. 2) shows the beginning of an obvious peak due to the enhancement of SM (from 173 g/cm^3) in region B. Furthermore, we compared variations in difference in passive microwave brightness temperature and SM in the two regions to understand the relationship between SM and brightness temperature using daily area-averaged data for the period 2008–2010 (see Fig. 3). Considering the influence of water vapor at frequencies 22 GHz and 91 GHz [19], [25], only 19 GHz and 37 GHz in horizontal and vertical polarizations (19H, 19V, 37H and 37V) were analyzed. The difference in brightness temperatures in Fig. 3 was computed using the brightness temperature over region B minus the brightness temperature over region A. The difference in SM was also computed using

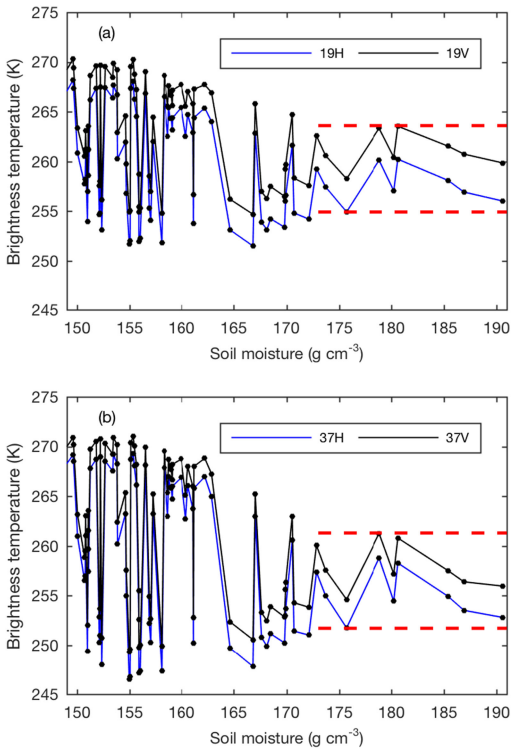

Fig. 4. Difference in the SM and in passive microwave brightness temperature in region B using daily three-year area-averaged data during 2008–2010. (a) 19 GHz with horizontal and vertical polarizations. (b) 37 GHz with horizontal and vertical polarizations. The part between the two horizontal red dash lines showing smaller fluctuations.

the SM over region B minus the SM over region A, as shown in Fig. 3. We have observed a completely opposite variation trend (the distinct trough in the difference of brightness temperature corresponds to the distinct peak in the difference of SM) on the difference of brightness temperature when the difference of SM reached to the maximum peak (see the variations between the two black dash lines in Fig. 3). From Fig. 2, we can easily find an abrupt increase in difference in SM, caused by the enhancement of SM in region B, which indicated the brightness temperature over region B decreased once the SM value is higher compared with a certain value (see Fig. 3). Liquefaction and water ejection phenomena associated with the Wenchuan and Lushan earthquakes occurred in region B have also been reported based on field investigations [26], [27], which could further increase SM.

We have also analyzed the area-averaged microwave brightness temperature variations at 19 GHz and 37 GHz with the area-averaged SM in region B based on the daily three-year area-averaged data for the period 2008–2010 (see Fig. 4). It clearly shows smaller fluctuations in microwave brightness temperature when the SM value is greater than 173 g/cm^3 at both 19 GHz and 37 GHz (see the part between the two horizontal red dash lines in Fig. 4). Correspondingly, the red shadow region in Fig. 2 shows the SM value range with smaller fluctuations of brightness temperature. Considering the variations in microwave brightness temperature in two different SM regions, different thresholds are considered for the two regions. To identify the possible microwave radiation signals associated with earthquake activities, lower threshold is set in the high SM region with the smaller fluctuations on brightness temperature. The potential seismic signals could be mistakenly deleted caused by setting high threshold in the high-SM region. Also, the threshold may vary from one location to other locations, depending on the soil thickness, geology, ground water and SM regime, and several other factors.

According to the detailed analysis mentioned above, we have considered setting different threshold values for different SM regions in order to detect potential abnormal signals associated with strong earthquakes using passive microwave brightness temperature data. In high-SM region, microwave brightness temperature variations show pronounced decline when SM has high values (see Fig. 4). If we set the same threshold as the low-SM region, the possible abnormal signals associated with the earthquake activities occurred in high-SM region may likely to be missed due to its small variations in microwave brightness temperature. A smaller threshold value of abnormal signals extraction associated with the earthquakes should be considered in the area with high SM compared with low SM.

B. Segmented Threshold Method

For lower SM regions, the IMRA is proposed to detect possible seismic signals [19]. As discussed in Section II-A, different threshold values should be considered for the frequently occurring earthquake regions with different SM environments due to the influence of SM on microwave brightness temperature. In this article, an improved IMRA based on segmented threshold method has been proposed.

First, the brightness temperature data on a specific region obtained in the years in the absence of strong earthquakes are selected as background value. The reference fields for the temporal mean $\mu_{T_{f(p,t)}}$ and the temporal standard deviation $\delta_{T_{f(p,\ t)}}$ were computed using these background values, which reflect the natural variability of brightness temperature. $\mu_{T_f(p,t)}$ and $\delta_{T_f(p,t)}$ are defined as follows:

$$\mu_{T_f(p,t)} = \frac{\sum_{i=1}^{N} T_f\,(p,t)}{N} \tag{1}$$

$$\delta_{T_f(p,t)} = \sqrt{\frac{1}{N-1}\sum_{i=1}^{\mathrm{N}} \left|T_f\,(p,t) - \mu_{T_f(p,t)}\right|^2} \tag{2}$$

where $T_f(p,t)$ is the brightness temperature at the frequency $f(\mathrm{GHz})$, the time t, and the pixel p. t represents the same time (one day, five days, or others) for difference years. N is the number of years of background data. $\mu_{T_f(p,t)}$ and $\delta_{T_f(p,t)}$, respectively, are the mean value and the standard deviation of brightness temperature for the time t, over the pixel p at the frequency f (GHz).

The selected region is divided according to varying SM. The determination of the segmentation threshold (St) value and the IMRA anomalies detection threshold (Dt) value are considered based on the relationship between SM and microwave brightness temperature, as discussed in Section II-A and also in our earlier work [19] for low-SM region. For the region with SM greater than or equal to threshold value (SM $\geq$ St), lower IMRA

anomalies Dt value is considered, and the region with low SM (SM < St) is set as higher IMRA anomalies Dt value. IMRA for the time t and the pixel p at the frequency f (GHz) is represented by the function $\mathrm{S}_f(p,t)$, which is given as

$$S_f\,(p,t) = \frac{T_f\,(p,t) - \mu_{T_f(p,t)}}{\mathrm{Dt} \times \delta_{T_f(p,t)}} \tag{3}$$

where

$$\mathrm{Dt} = \begin{cases} 4, & \mathrm{SM} < \mathrm{St} \\ 1, & \mathrm{SM} \geq \mathrm{St}. \end{cases}$$

Dt = 4 is based on our analysis on the earthquakes occurred in the low-SM region using SSM/I brightness temperature data [19]. According to the analysis of the relationship between SM and microwave brightness temperature in regions A and B (see Figs. 2–4), SM of 173 g/cm^3 was considered as the St value. The area with SM greater than or equal to 173 g/cm^3 was set as low IMRA anomalies Dt value (Dt = 1), whereas the area with SM less than 173 g/cm^3 was set as high IMRA anomalies Dt value (Dt = 4).

In the present article, we have considered five-day average microwave brightness and SM data to avoid coverage gaps due to coverage of polar orbiting satellite, as discussed in our earlier study [19]. Furthermore, we have considered descending mode (nighttime) data to avoid the influence of the sunlight and human activities during daytime. Thus, a total of 73 five-day average data were obtained for one year to ensure coverage. Naming convention for data is according to the last day of all used data for average. For example, 2008-050D.37H means the average of microwave brightness temperature at 37 GHz with horizontal polarization from 46 to 50 Julian days of 2008, where D represents descending mode.

III. Case Studies

Considering the time availability periods for DMSP F17 SSMIS data [28], besides the 2008 Wenchuan earthquake, the other two strong earthquakes (the Lushan and the Jiuzhaigou earthquakes) with magnitude greater than 6.5 occurred in the high-SM region of Sichuan province, China, during 2008—2018 have been analyzed in the present study (see Fig. 1). The F17 SSMIS brightness temperature data during the years 2009, 2011, and 2015 in the absence of strong earthquakes ($M > 5.0$) were selected to compute background values for comparison.

A. 2008 Wenchuan ($M = 7.8$) Earthquake

The deadly Wenchuan earthquake generated about 300-km long rupture zone along the Longmenshan (LMS) thrust belt located in the eastern margin of the Tibetan Plateau [29]. The segmented threshold method described in Section II-B has been used to compute IMRA and detect anomalous variations associated with this earthquake event.

Fig. 5 shows spatial variations of IMRA at 37 GHz with horizontal polarization around the Wenchuan earthquake. The main earthquake occurred on the 133 Julian day (12 May) of 2008. An increase in IMRA is observed along the LMS fault zone during the 61–65 Julian days of the year 2008. The next high

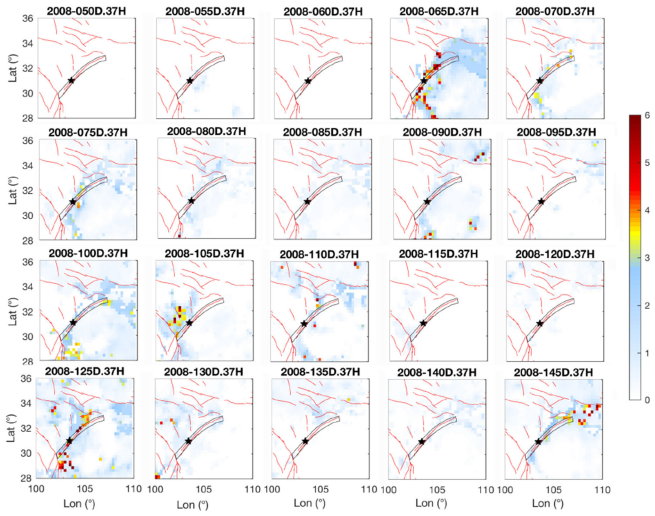

Fig. 5. Spatial distribution of IMRA at 37 GHz horizontal polarization during 46–145 days of 2008 around the Wenchuan ($M = 7.8$) earthquake based on five-day average microwave brightness temperature data. Star represents the location of epicenter, and red lines indicate main active faults. The region bounded by the black lines shows the fault zone used to compute temporal variations in IMRA.

IMRA appeared 8–12 days prior to the main earthquake event (the 121–125 Julian days), along the LMS fault zone and near to the epicenter. Afterward, the IMRA decreased gradually. The earliest increased microwave brightness temperature was detected about two months prior to the Wenchuan earthquake compared with other geophysical, geochemical, and atmospheric parameters (outgoing longwave radiation, surface latent heat flux, air temperature, skin temperature, atmospheric aerosol optical depth and CH_4, CO), as observed by others [16], [21], [22], [30], [31]. The spatial variations of IMRA at 19 GHz with horizontal and vertical polarizations, 37 GHz with vertical polarization, and 91 GHz with horizontal and vertical polarizations around the Wenchuan earthquake are shown in Supplementary Fig. S1, and no more obvious increase in IMRA was observed during this period compared with 37 GHz horizontal polarization.

B. 2013 Lushan ($M = 6.6$) Earthquake

On April 20, 2013, another strong earthquake with magnitude 6.6 occurred in Lushan, Sichuan province, China. This earthquake occurred on the southern segment of LMS fault (epicenter 30.308°N, 102.888°E, source: USGS) located about 80 km southwest of the 2008 Wenchuan earthquake (see Fig. 1). Similar to the Wenchuan earthquake, it was also caused by the southeast movement of Bayan Har tectonic block to the LMS tectonic belt as well as the collision and compression between the blocks [32]. Field investigations indicated that no obvious earthquake surface rupture generated and the seismogenic fault was a blind reverse fault [32]. The sharp variations of water radon and water level have been observed about one week prior to this earthquake [33].

Fig. 6 shows the spatial distribution of IMRA at 37 GHz horizontal polarization around the Lushan earthquake that occurred on the 110 Julian day of 2013. The slight enhanced IMRA appeared during the 51–55 Julian days (about two months

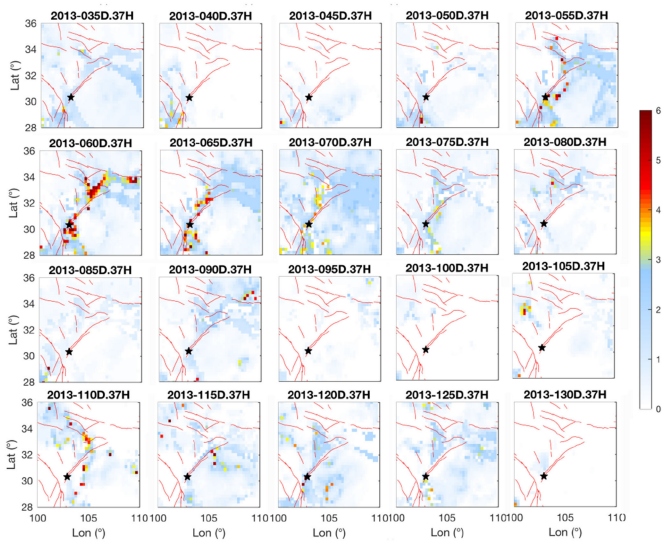

Fig. 6. Spatial distribution of IMRA at 37 GHz horizontal polarization during 31–130 Julian days of 2013 around the Lushan ($M = 6.6$) earthquake based on five-day average microwave brightness temperature data. Star represents the location of epicenter. Red lines indicate main active faults.

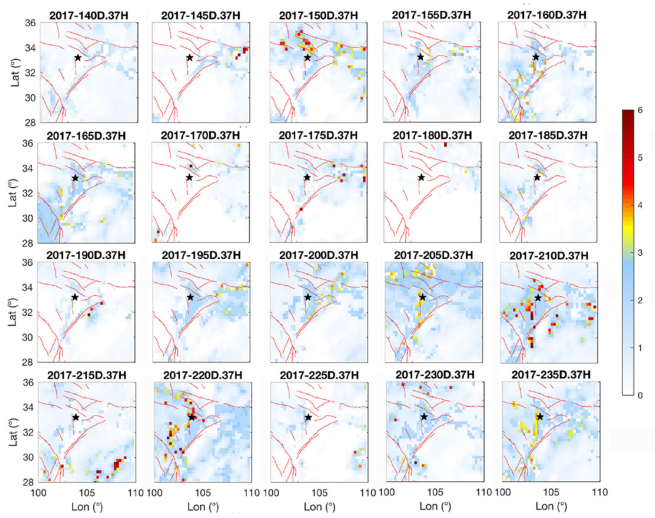

Fig. 7. Spatial variations of IMRA at 37 GHz horizontal polarization for the period 136–235 days of 2017 around the Jiuzhaigou ($M = 6.5$) earthquake based on five-days average microwave brightness temperature data. Star represents the location of epicenter. Red lines indicate main active faults.

prior to the main earthquake event) and located around the impending epicenter. An enhancement in IMRA was observed along the LMS fault zone and continued around the epicenter during the 56–60 Julian days, afterward IMRA decreased during the 61–65 Julian days. The high values around epicenter were observed to be persistent for about two weeks. Different from the Wenchuan earthquake, high value of the IMRA was not observed prior to the impending earthquake. It is difficult to understand high and low values of IMRA in cases of the Wenchuan and the Lushan earthquakes, and such contrasting difference was observed in radon concentration trends in case of these two earthquakes [33]. No unusual IMRA variations were observed at 19 GHz horizontal and vertical polarizations, 37 GHz vertical polarization, and 91 GHz horizontal and vertical polarizations (see Supplementary Fig. S2).

C. 2017 Jiuzhaigou ($M = 6.5$) Earthquake

On August 8, 2017 (the 220 Julian day), the Jiuzhaigou earthquake ($M = 6.5$) occurred on the intersection area of three faults (Tazang, Minjiang, and Huya faults) in the eastern part of the Tibetan Plateau, China [34] (see Fig. 1). No surface rupture was observed during field investigation. It is presumed that the seismogenic fault of this earthquake lies in the northern segment of Huya fault [35]. The results based on InSAR and GPS observations show triggering of the earthquake associated with a blind fault with a length of about 23 km [34].

The apparent enhancements in IMRA were observed at 37 GHz horizontal polarization (see Fig. 7) compared with 19 GHz horizontal and vertical polarizations, 37 GHz vertical polarization, and 91 GHz horizontal and vertical polarizations (see Supplementary Fig. S3). As shown in Fig. 7, an increased IMRA occurred during the 146–150 Julian days (more than two months prior to the main earthquake event) and located in the north side of the future epicenter and distributed along the NW-striking faults. Afterward, higher IMRA value appeared again and distributed on the faults around the epicenter of the earthquake during the 206–210 Julian days (two weeks prior to the main earthquake event). An enhancement in IMRA on the epicentral area appeared prior to the impending earthquake during the 216–220 Julian days. Unlike the enhanced IMRA distributed on the seismogenic fault for the other two earthquakes, the spatial variations of enhanced IMRA prior to the Jiuzhaigou earthquake mainly distributed around the surrounding faults and were concentrated in the epicentral area until the occurrence of the main earthquake event.

IV. Validation

In order to confirm the unique IMRA variations (discussed in Section III) related to earthquake activities, we computed the IMRA values during the years 2008–2018. The accumulated IMRA value has been considered to study the long-term variations in microwave brightness temperature over the fault zone and epicentral region. In addition, eight-day average brightness temperature data have been considered to verify that the enhanced IMRA obtained using the five-day average data are not the random noise caused by the change of solar angle. According to the results presented in Section III, only IMRA values at 37 GHz horizontal polarization were considered for validation.

A. Long-Term Time Series Variations of Accumulated IMRA Value

1) Wenchuan M 7.8 and the Lushan M 6.6 Earthquakes: Both the epicenters of the 2008 Wenchuan M 7.8 and the 2013 Lushan M 6.6 earthquakes are located on the LMS fault zone. Compared with Wenchuan earthquake that occurred on the mid-section of LMS fault belt, the seismogenic fault of the Lunshan earthquake is a blind thrust fault located on the southern section of the LMS fault belt. The same area over LMS thrust fault (the area

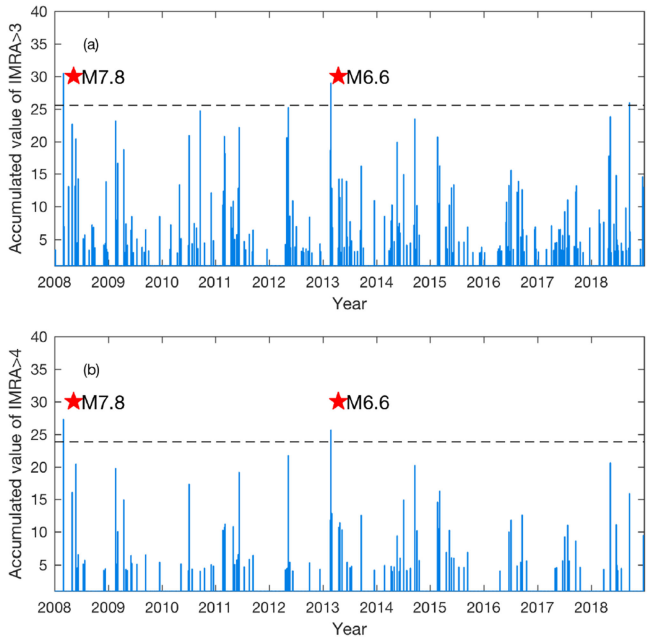

Fig. 8. Temporal variations of accumulated IMRA at 37 GHz horizontal polarization over LMS fault during 2008–2018. (a) IMRA > 3. (b) IMRA > 4. Black dash line represents the mean value plus 3.0 standard deviations. Red stars show the 2008 Wenchuan and the 2013 Lushan earthquakes.

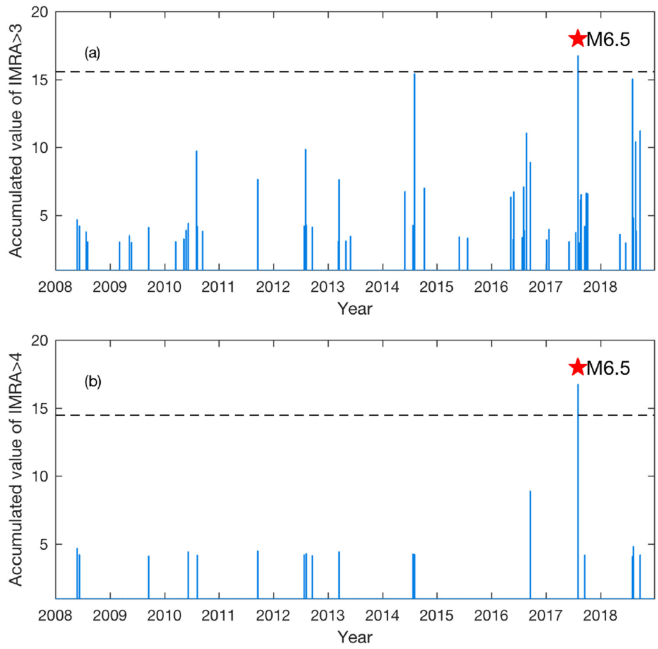

Fig. 9. Temporal variations of IMRA at 37 GHz horizontal polarization over the epicentral region of the Jiuzhaigou earthquake for the periods 2008-2018. (a) IMRA > 3. (b) IMRA > 4. Black dash line represents the mean value plus 3.0 standard deviations. Red stars show the 2017 Jiuzhaigou earthquake.

bounded by black lines in Fig. 5) is considered here to analyze the temporal variations of IMRA for the two strong earthquakes. The accumulated IMRA values over the region during 2008–2018 have been computed to study the long-period variations. The accumulated IMRA is defined as $\sum S_f(p,t)$. Those values of IMRA < 3 have not been considered when we computed the accumulated IMRA to avoid interference of the slight changes in microwave brightness temperature.

Fig. 8(a) shows the temporal variations of accumulated value of IMRA > 3 during the period 2008–2018 over LMS fault zone. Furthermore, we set the threshold value as the mean value of 11 years (2008–2018) plus 3.0 standard deviations. The highest (30.49) and the second highest (29.00) accumulated IMRA values exceed the threshold line with the value of 25.56 [see the black dash line in Fig. 8(a), the mean value is 8.04, and the standard deviation is 5.84] appeared prior to the 2008 Wenchuan ($M = 7.8$) and the 2013 Lushan ($M = 6.6$) earthquakes, respectively. In addition, the accumulated values of IMRA > 4 during this period were computed. Only the two distinct enhancements exceeded the threshold value of 23.84 (see the black dash line in Fig. 8(b), the mean value is 8.24, and the standard deviation is 5.20) appeared prior to the two strong earthquakes, respectively [see Fig. 8(b)]. The long-period variations of 11 years clearly show enhanced IMRA over the LMS thrust fault showing close correlation with strong earthquake activities.

2) Jiuzhaigou M 6.5 Earthquake: Considering the seismogenic fault of the 2017 Jiuzhaigou earthquake (blind fault) [34], the epicentral region (2 pixel $\times$ 2 pixel, that is, 50 km $\times$ 50 km) is considered to analyze the temporal variations of microwave brightness temperature. Similar to the analysis associated with the Wenchuan and the Lushan earthquakes, the accumulated IMRA variations during the period 2008–2018 using IMRA > 3 and IMRA > 4 have been computed, respectively. The threshold value was also set as the mean value of 11 years plus 3.0 standard deviations. As shown in Fig. 9, the highest accumulated IMRA value of 16.75 appeared on the occurrence of the earthquake, which is greater than the threshold value of 15.55 (the mean value is 5.65 and the standard deviation is 3.30) for using IMRA $>$ 3 [see Fig. 9(a)] and 14.47 (the mean value is 5.26 and the standard deviation is 3.07) for using IMRA > 4 [see Fig. 9(b)]. In Fig. 9(a), we can see other two high accumulated values of 15.42 and 15.03 in the years 2014 and 2018 (not exceeding the threshold line). However, when we set IMRA > 4, a more obvious accumulated IMRA peak appeared on the occurrence of the main earthquake event [see Fig. 9(b)].

B. Spatial Variations of Eight-Day Average IMRA Value

To make sure the IMRA variations based on the five-day average data are not caused by the change of solar angle, the eight-day average brightness temperature data have also been considered. Figs. 10–12 show the spatial variations of IMRA around the three strong earthquakes using eight-day average microwave brightness temperature data. For the 2008 Wenchuan earthquake, the enhanced IMRA along the LMS fault appeared during the 63–72 and 121–128 Julian days of 2008 (see Fig. 10), compared with the enhanced IMRA on the 61–65 and 121–125 Julian days of 2008 based on the five-day average brightness temperature data (see Fig. 5). For the 2013 Lushan earthquake, the IMRA enhanced during the 57–64 Julian days of 2013 using 8-day average data (see Fig. 11) and the 51–65 Julian days using five-day average data (see Fig. 6). We can easily find a

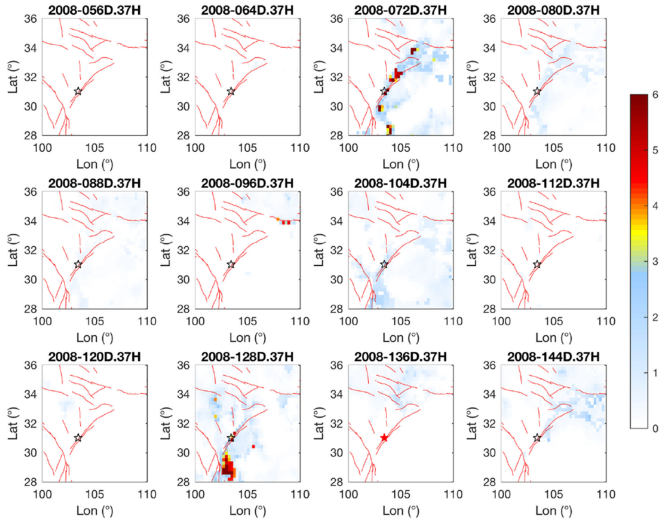

Fig. 10. Spatial distribution of IMRA at 37 GHz horizontal polarization around the 2008 Wenchuan ($M = 7.8$) earthquake based on eight-day average microwave brightness temperature data. Star represents the location of epicenter. Red lines indicate main active faults. The image with red star shows eight-day average that include the day of the main event.

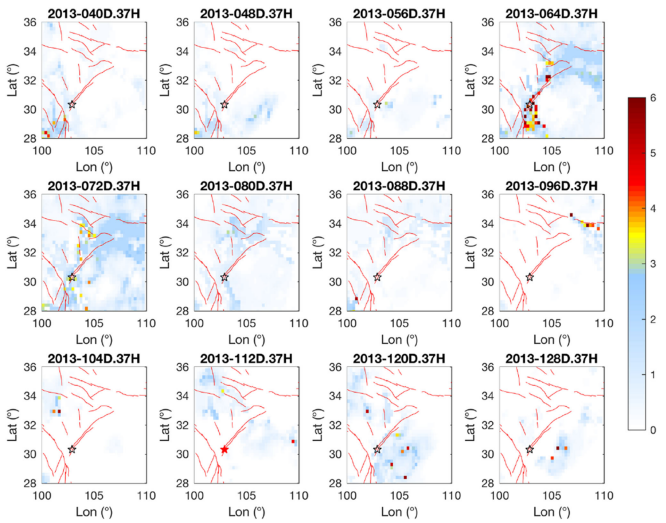

Fig. 11. Spatial distribution of IMRA at 37 GHz horizontal polarization around the 2013 Lushan ($M = 6.6$) earthquake based on eight-day average microwave brightness temperature data. Star represents the location of epicenter. Red lines indicate main active faults. The image with red star shows the eight-day average that include the day of the main shock.

good agreement in the enhanced IMRA temporal and spatial distributions for the Wenchuan and the Lushan earthquakes on both five- and eight-day average datasets.

However, for the Jiuzhaigou earthquake, the earliest enhanced IMRA distributed on the faults in the northwest of the epicenter during the 145–152 Julian days of 2017 based on eight-day average data (see Fig. 12), and the IMRA variations located on the faults in the north of the epicenter during 146–150 Julian days based on five-day average data (see Fig. 7). Besides, the magnitude of enhanced IMRA during the 201–208 Julian days (using eight-day average data) is observed to be less than the variations occurred during 206–210 Julian days (using five-day

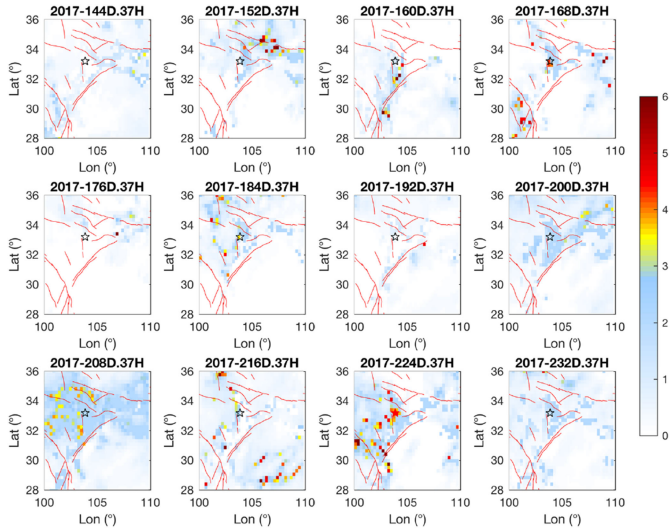

Fig. 12. Spatial distribution of IMRA at 37 GHz horizontal polarization around the 2017 Jiuzhaigou ($M = 6.5$) earthquake based on eight-day average microwave brightness temperature data. Star represents the location of epicenter. Red lines indicate main active faults. The image with red star shows the eight-day average that include the day of the main shock.

average data). The variations during the 216–220 Julian days (see Fig. 7) are similar to the variations during the 217–224 Julian days (see Fig. 12). The slight difference could be due to the missing or weakened signals caused by more data for averaging.

The results of comparative analysis based on five- and eight-day average data show that the enhanced IMRA variations distributed along the fault zone and around the epicenter, detected using the segmented threshold method, were not coming from the random noise caused by the change of solar angel on different days.

V. Discussion

A. Influence of Earthquake Activities on Enhanced IMRA Spatial Distribution

The enhanced IMRA reflects thermal effect associated with tectonic activities, which could be due to the accumulated stress in the seismogenic region. Before the occurrence of earthquakes, subsurface or surface thermal effects could generate due to the release of underground gases and vapors, electrical and electromagnetic radiations, or the combinations of these factors. Fig. 13 shows the detailed spatial distribution of IMRA enhancement based on five-day microwave brightness temperature data at 37 GHz horizontal polarization before the three strong earthquakes. It shows that the IMRA variations strongly depend on the seismic and tectonic activities. For the Wenchuan [see Fig.13(a) and (b) corresponds to the subfigures titled with 065 and 125 in Fig. 5] and the Lushan earthquakes [Fig.13(c) and (d) corresponds to the subfigures titled with 060 and 065 in Fig. 6] that occurred on the LMS fault zone, the enhanced IMRA mainly distributed along the fault with the NE direction. The enhanced IMRA was located on the north and south sections of LMS fault two months prior to the Wenchuan earthquake [see Fig. 13(a)] and moved to the epicenter about one week prior to the main

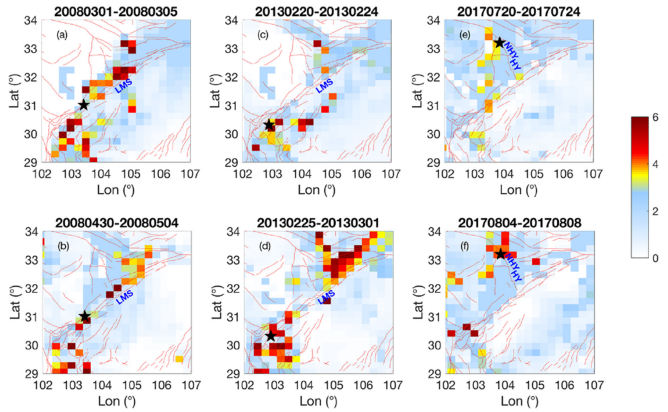

Fig. 13. Spatial distributions of enhanced IMRA at 37 GHz horizontal polarization before three strong earthquakes. (a) and (b) Wenchuan. (c) and (d) Lushan. (e) and (f) Jiuzhaigou. Black stars represent the location of epicenters. Red lines show the detailed active faults. LMS—Longmenshan fault; NHY—Northern Huya fault; HY—Huya fault.

earthquake event [see Fig. 13(b)]. For the Lushan earthquake, the enhanced IMRA appeared continuously around the epicenter about two months before the main event [see Fig.13(c) and (d)].

However, the Jiuzhaigou earthquake was inferred to be caused by a blind NNW-trending strike–slip fault—the Northern Huya fault [34], [36]. The enhanced IMRA shown in Fig.13(e) and (f) (correspond to the subfigures titled with 205 and 220 in Fig. 7) does not provide any information about the seismogenic fault but mainly distributed on the surrounding faults that are exposed to the surface and the region around the epicenter. And the magnitude of enhanced IMRA increased around the epicenter prior to the impending earthquake.

We have also observed differences on the enhanced IMRA for the Wenchuan and the Lushan earthquakes, both occurred along the LMS fault. The enhanced IMRA around the epicentral region appeared about two months prior to the Lushan earthquake and only two weeks prior to the Wenchuan earthquake [the enhanced IMRA appeared two months before the Wenchuan earthquake distributed along LMS fault, but did not appear around the epicentral region, Fig. 13(a) and (b)]. The possible reason could be due to a large number of fractures caused by the Wenchuan great earthquake along the LMS fault through which gas emitted prior to the Lushan earthquake [30]. The similarity in temporal–spatial distribution of enhanced microwave brightness temperature observed by SSMIS and strong CH_4 emissions observed by the Atmospheric Infrared Sounder (AIRS) onboard AQUA satellite show a good correlation [see Figs.13(c) and (d) and 14]. Cui *et al*. [30] showed that the earliest CH_4 anomalies around the Lushan earthquake epicenter appeared on February 3–10, 2013 [see Fig. 14(a)]. After ten days, microwave brightness temperature was enhanced [see Fig. 13(c)]. The CH_4 anomalies appeared again during February 19–March 6, 2013, and moved from the epicentral region to the north and south sides of the LMS fault zone [see Fig. 14(b) and (c)]. Similar variations in microwave brightness temperature have been observed during this period [see Fig. 13(d)]. The difference in spatial scales of microwave brightness temperature and CH_4 anomalies could be due to the difference in spatial resolutions of two datasets (25 km for microwave brightness temperature and 1.0° for CH_4).

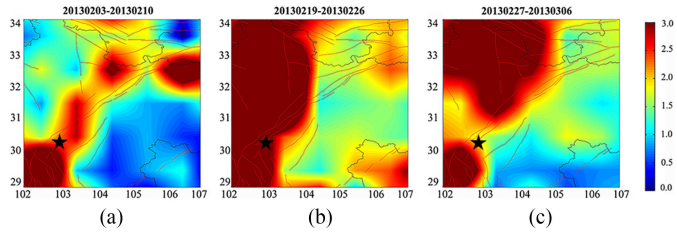

Fig. 14. Spatial distributions of eight-day nighttime total column of CH_4 anomalies observed from AQUA AIRS prior to the Lushan Earthquake. (a) February 3–10, 2013. (b) February 19–26, 2013. (c) February 27–March 6, 2013. Black star shows the epicenter of the Lushan earthquake. Red lines show the main active faults.

B. Comparison With the Results of the Earthquakes Occurred in Low-SM Region

In the present study, the spatial and temporal characteristics for the three earthquakes are consistent with the results associated with the 1997 Manyi M 7.5 earthquake and the 2001 Kokoxili M 7.8 earthquake [19], which clearly provide confidence that the segmented threshold method proposed in this article is feasible for the earthquakes occurred in the region with high SM. However, by analyzing the variations of IMRA at 19 GHz and 37 GHz (see Supplementary Figs. S1–S3), 37 GHz seems to be an important frequency to detect the unusual thermal signals associated with strong earthquakes in high-SM region compared with 19 GHz that looks to be a potential frequency for the low-SM environment. We have also analyzed the influence of different parameters on microwave brightness temperature in different underlying areas [24]. In high-SM region, the effect of SM on brightness temperature at 19 GHz and 37 GHz with horizontal polarization is smaller in comparison with other frequencies. In addition, brightness temperature at 37 GHz shows a higher correlation with skin temperature compared with 19 GHz in high-SM region. This could explain why 37 GHz with horizontal polarization has a better response to the earthquake events occurred in high-SM region. In addition, considering the possible impact of clouds and rain in the sky at 37 GHz, we have also considered the precipitation rate and cloud fraction during the periods of enhanced IMRA prior to the three earthquakes based on five-day average (corresponding to five-day average IMRA variations) The Tropical Rainfall Measuring Mission (TRMM) precipitation rate and AIRS cloud fraction data (see supplementary Figs. S4–S6). The results show no obvious correlation between the spatial distributions of unusual IMRA variations and high values of precipitation rate and cloud fraction prior to the three earthquakes. The spatial variations of enhanced IMRA observed in this article are irrelevant to the weather conditions. Similar characteristics of microwave signals have also been observed in the case of 2015 Nepal ($M = 7.8$) earthquake and its strong aftershock ($M = 7.3$) that occurred in high-SM region using the improved IMRA [37].

VI. Conclusion

In the present article, the effect of SM on microwave brightness temperature has been considered for the first time to detect the possible microwave radiation variations associated with the strong earthquake activities occurred in high-SM region.

The three great earthquakes occurred in Sichuan province, China, during 2008–2018 have been analyzed based on IMRA computed by the segmented threshold method using DMSP F17 SSMIS microwave brightness temperature data. The enhancements in IMRA over the main fault and the region surrounding the epicenter have been observed prior to the three strong earthquakes. Nevertheless, it could be difficult to have quantitative evaluation associated with the earthquake activities due to infrequent earthquake activities in the same region with similar earthquake characteristics, although the enhanced microwave radiations have been observed prior to the earthquakes along the main fault, which is related to the thermal anomalies caused by the stress concentration during the earthquake preparation period. The results discussed here show the maximum variations of IMRA prior to the strong earthquakes over a long period along the active tectonic zone, and further research will help to develop quantitative and qualitative evaluations of early detection of potential earthquake anomalies in the higher SM environment. It should also be noted that the determination of the St value is based on the analysis of the relationship between SM and brightness temperature in the specific regions proposed in this article, which may need to be adjusted when segmented threshold method is applied to other high-SM regions to detect thermal anomaly signals associated with earthquakes.

ACKNOWLEDGMENT

The authors would like to thank NASA National Snow and Ice Data Center Distributed Active Archive Center for providing DMSP SSMIS brightness temperature and AMSR-E soil moisture data. The TRMM and AIRS satellite data products used in this study were available through NASA Giovanni portal, and authors would like to thank NASA Giovanni team for their efforts. The authors would also like to thank the editor and the four anonymous referees for their comments/suggestions that have helped them to improve earlier version of the manuscript.

REFERENCES

[1] V. I. Gornyi, A. G. Sal'Man, A. A. Tronin, and B. V. Shilin, "Outgoing infrared radiation of the earth as an indicator of seismic activity," *Doklady Akademii Nauk SSSR*, vol. 301, pp. 67–69, 1988.

[2] A. Tronin, "Satellite thermal survey—A new tool for the study of seismoactive regions," *Int. J. Remote Sens.*, vol. 17, no. 8, pp. 1439–1455, 1996.

[3] A. A. Tronin, M. Hayakawa, and O. A. Molchanov, "Thermal IR satellite data application for earthquake research in Japan and China," *J. Geodyn.*, vol. 33, no. 4/5, pp. 519–534, 2002.

[4] D. Ouzounov, and F. Freund, "Mid-infrared emission prior to strong earthquakes analyzed by remote sensing data," *Adv. Space Res.*, vol. 33, no. 3, pp. 268–273, 2004.

[5] F. Jing, H. Wang, S. Hong, and Y. Dong, "Thermal infrared variation associated with strong earthquakes in Xinjiang using satellite data," in *Proc. IEEE Int. Geosci. Remote Sens. Symp.*, 2016, pp. 2865–2868.

[6] C. Aliano, R. Corrado, C. Filizzola, N. Genzano, N. Pergola, V. Tramutoli, "Robust TIR satellite techniques for monitoring earthquake active regions: Limits, main achievements and perspectives," *Ann. Geophys.*, vol. 51, no. 1, pp. 303–317, 2008.

[7] V. Tramutoli *et al.*, "On the possible origin of thermal infrared radiation (TIR) anomalies in earthquake-prone areas observed using robust satellite techniques (RST)," *Chem. Geol.*, vol. 339, no. 2, pp. 157–168, 2013.

[8] K. Qin, L. Wu, S. Zheng, and W. Ma, "Discriminating satellite IR anomalies associated with the MS 7.1 Yushu earthquake in China," *Adv. Space Res.*, vol. 61, no. 5, pp. 1324–1331, 2018.

[9] N. Ahmad *et al.*, "Investigation of spatio-temporal satellite thermal IR anomalies associated with the Awaran earthquake (Sep 24, 2013; M 7.7), Pakistan," *Pure Appl. Geophy.*, vol. 176, no. 8, pp. 3533–3544, 2019.

[10] L. Piroddi and G. Ranieri, "Night thermal gradient: A new potential tool for earthquake precursors studies. An Application to the Seismic Area of L'Aquila (Central Italy)," *IEEE J. Sel. Topics Appl. Earth Observ. Remote Sens.*, vol. 5, no. 1, pp. 307–312, Feb. 2012.

[11] M. Lisi, C. Filizzola, N. Genzano, R. Paciello, N. Pergol, and V. Tramutoli, "Reducing atmospheric noise in RST analysis of TIR satellite radiances for earthquakes prone areas satellite monitoring," *Phys. Chem. Earth, A/B/C*, vol. 85/86, pp. 87–97, 2015.

[12] K.-I. Maki, T. Takano, E. Soma, K. Ishii, S. Yoshida, and M. Nakatani, "An experimental study of microwave emission from compression failure of rocks," *J. Seismological Soc. Jpn.*, vol. 58, no. 4, pp. 375–384, 2006.

[13] S. Liu, Z. Xu, J. Wei, J. Huang, and L. Wu, "Experimental study on microwave radiation from deforming and fracturing rock under loading outdoor," *IEEE Trans. Geosci. Remote Sens.*, vol. 54, no. 9, pp. 5578–5587, Sep. 2016.

[14] T. Maeda and T. Takano, "Detection algorithm of earthquake-related rock failures from satellite-borne microwave radiometer data," *IEEE Trans. Geosci. Remote Sens.*, vol. 48, no. 4, pp. 1768–1776, Sep. 2010.

[15] Y. Jie and G. Guangmeng, "Preliminary analysis of thermal anomalies before the 2010 Baja California M7.2 earthquake," *Atmósfera*, vol. 26, no. 4, pp. 473–477, 2013.

[16] R. P. Singh, W. Mehdi, R. Gautam, J. S. Kumar, J. Zlotnicki, and M. Kafatos, "Precursory signals using satellite and ground data associated with the Wenchuan earthquake of 12 May 2008," *Int. J. Remote Sens.*, vol. 31, no. 13, pp. 3341–3354, 2010.

[17] T. Maeda and T. Takano, "Detection of microwave signals associated with rock failures in an earthquake from satellite-borne microwave radiometer data," in *Proc. IEEE Int. Geosci. Remote Sens. Symp.*, 2009, vol. 3 pp. III-I61–III-64, https://ieeexplore.ieee.org/document/5418159/citations#citations.

[18] T. Takano and T. Maeda, "Experiment and theoretical study of earthquake detection capability by means of microwave passive sensors on a satellite," *IEEE Trans Geosci. Remote Sens.*, vol. 6, no. 1, pp. 107–111, Jan. 2009.

[19] F. Jing, R. P. Singh, K. Sun, and X. Shen, "Passive microwave response associated with two main earthquakes in Tibetan Plateau, China," *Adv. Space Res.*, vol. 62, no. 7, pp. 1675–1689, 2018.

[20] Y. S. Zhang, X. Guo, M. Zhong, W. Shen, W. Li, and B. He, "Wenchuan earthquake: Brightness temperature changes from satellite infrared information," *Chin. Sci. Bull.*, vol. 55, no. 18, pp. 1917–1924, 2010.

[21] F. Jing, X. H. Shen, C. L. Kang, and P. Xiong, "Variations of multiparameter observations in atmosphere related to earthquake," *Natural Hazards Earth Syst. Sci.*, vol. 13, no. 1, pp. 27–33, 2013.

[22] L. Wu, K. Qin, and S. Liu, "GEOSS-based thermal parameters analysis for earthquake anomaly recognition," *Proc. IEEE*, vol. 100, no. 10, pp. 2891–2907, Oct. 2012.

[23] D. Ouzounov, S. Habib, and S. Ambrose, "Multisensor approach analyzing atmospheric signals for possible earthquake precursors. Application of remote sensing for risk management," in *Risk Wise*. Cham, Switzerland: Tudor Rose, 2008, pp. 162–165.

[24] F. Jing and R. P. Singh, "Sensitivity of land covers on passive microwave brightness temperature," in *Proc. IEEE Int. Geosci. Remote Sens. Symp.*, 2019, pp. 9569–9572.

[25] S. Dey, S. Sarkar, and R. P. Singh, "Anomalous changes in column water vapor after Gujarat earthquake," *Adv. Space Res.*, vol. 33, no. 3, pp. 274–278, 2004.

[26] J. L.-Zeng *et al.*, "Liquefaction in western Sichuan Basin during the 2008 Mw 7.9 Wenchuan earthquake, China," *Tectonophysics*, vol. 694, pp. 214–238, 2017.

[27] Z. Shi, G. Wang, C.-.. Wang, M. Manga, and C. Liu, "Comparison of hydrological responses to the Wenchuan and Lushan earthquakes," *Earth Planet. Sci. Lett.*, vol. 391, pp. 193–200, 2014.

[28] D. Cavalieri, C. Parkinson, P. Gloersen, and H. Zwally, "Sea ice concentrations from Nimbus-7 SMMR and DMSP SSM/I-SSMIS passive microwave data," NASA DAAC at the National Snow and Ice Data Center, Boulder, CO, USA, vol. 25, 1996.

[29] X. Xu *et al.*, "Coseismic reverse-and oblique-slip surface faulting generated by the 2008 Mw 7.9 Wenchuan earthquake, China," *Geology*, vol. 37, no. 6, pp. 515–518, 2009.

[30] Y. Cui *et al.*, "Satellite observation of CH4 and CO anomalies associated with the Wenchuan MS 8.0 and Lushan MS 7.0 earthquakes in China," *Chem. Geol.*, vol. 469, pp. 185–191, 2017.
[31] K. Qin, L. X. Wu, S. Zheng, Y. Bai, and X. Lv, "Is there an abnormal enhancement of atmospheric aerosol before the 2008 Wenchuan earthquake?," *Adv. Space Res.*, vol. 54, no. 6, pp. 1029–1034, 2014.
[32] X. Xu *et al.*, "Seismogenic structure of Lushan earthquake and its relationship with Wenchuan earthquake," *Earth Sci. Frontiers*, vol. 20, no. 3, pp. 11–20, 2013.
[33] Q. Ye, R. P. Singh, A. He, S. Ji, and C. Liu, "Characteristic behavior of water radon associated with Wenchuan and Lushan earthquakes along Longmenshan fault," *Radiat. Meas.*, vol. 76, pp. 44–53, 2015.
[34] S. Hong *et al.*, "Source model and stress disturbance of the 2017 Jiuzhaigou Mw 6.5 earthquake constrained by InSAR and GPS measurements," *Remote Sens.*, vol. 10, no. 9, 2018, Art. no. 1400.
[35] X. W. Xu *et al.*, "Discussion on seismogenic structure of Jiuzhaigou earthquake and its implication for current strain state in the southeastern Qinghai–Tibet plateau," *Chin. J. Geophys.*, vol. 60 no. 10, pp. 4018–4026, 2017.
[36] D. Zhao *et al.*, "InSAR and GPS derived coseismic deformation and fault model of the 2017 Ms7.0 Jiuzhaigou earthquake in the Northeast Bayanhar block," *Tectonophysics*, vol. 726, pp. 86–99, 2018.
[37] F. Jing, R. P. Singh, and X. Shen, "Land–atmosphere–meteorological coupling associated with the 2015 Gorkha (M 7.8) and Dolakha (M 7.3) Nepal earthquakes," *Geomatics, Natural Hazards Risk*, vol. 10, no. 1, pp. 1267–1284, 2019.

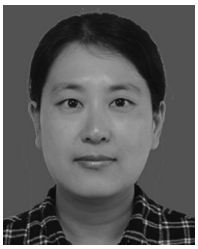

Feng Jing (Member, IEEE) was born in 1979. She received the B.S. degree in geology from the China University of Geosciences, Wuhan, China, in 2002, the M.E. degree in geophysical prospecting and information technology from the China University of Geosciences, Beijing, China, in 2005, and the Ph.D. degree in cartography and geographic information system from the Institute of Remote Sensing Applications, Chinese Academy of Science, in 2010.

She is currently an Associate Professor with the Institute of Earthquake Forecasting, China Earthquake Administration. She has authored two books and more than 20 papers. Her research interests include earthquake monitoring using remote sensing and lithosphere–atmosphere coupling associated with earthquakes.

Ramesh P. Singh (Member, IEEE) received the B.S., M.Sc., and Ph.D. degrees from Banaras Hindu University, India, in 1974, 1976, and 1980, respectively.

He is currently a Professor with the Schmid College of Science and Technology, Chapman University, Orange, CA, USA. He was a Professor with the Indian Institute of Technology, Kanpur, India, from 1986 to 2007, and with George Mason University, Fairfax, VA, USA, from 2003 to 2005 and also, from 2007 to 2009. He has authored more than 200 papers. His research interests include natural hazards, early warning of coastal earthquakes, soil moisture, landslides, snow avalanches, floods, dust storms, remote sensing applications, geophysical explorations, atmospheric pollution, and mining environment.

Dr. Singh is the Chief Editor for *Geomatics, Natural Hazards and Risk.*

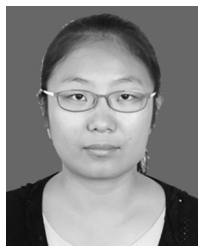

Yueju Cui was born in 1985. She received the B.S. degree in surveying and mapping from the Shijiazhuang University of Economics, China, in 2008, the M.E. degree from the Institute of Earthquake Forecasting, China Earthquake Administration, in 2011, and the Ph.D. degree in geochemistry from the China University of Geosciences, Beijing, China, 2014.

She is currently an Associate Professor with the Institute of Earthquake Forecasting, China Earthquake administration. She has authored 1 book and more than 10 papers. Her research interest includes gas geochemical changes based on satellite data.

Ke Sun received the B.S. and M.S. degrees in geographical information systems from Jilin University, China, in 2002 and 2007, respectively, and the Ph.D. degree in solid geophysics from the Institute of Geology, China Earthquake Administration, in 2017.

He is currently an Associate Professor with the Institute of Earthquake Forecasting, China Earthquake Administration. His research interest includes the application of space technology in earthquake prevention and disaster reduction.